Applied Catalysis B: Environmental 121–122 (2012) 95–104

Contents lists available at SciVerse ScienceDirect

Applied Catalysis B: Environmental

journal homepage: www.elsevier.com/locate/apcatb

Catalyst property of Co–Fe alloy particles in the steam reforming of biomass tar and toluene

Lei Wang[a], Yuji Hisada[a], Mitsuru Koike[a], Dalin Li[a], Hideo Watanabe[b], Yoshinao Nakagawa[a], Keiichi Tomishige[a,*]

[a] Department of Applied Chemistry, School of Engineering, Tohoku University, 6-6-07, Aoba, Aramaki, Aoba-ku, Sendai 980-8579, Japan
[b] Graduate School of Pure and Applied Sciences, University of Tsukuba, 1-1-1, Tennodai, Tsukuba, Ibaraki 305-8573, Japan

ARTICLE INFO

Article history:
Received 6 February 2012
Received in revised form 24 March 2012
Accepted 26 March 2012
Available online 2 April 2012

Keywords:
Cobalt
Iron
Alloy
Steam reforming
Biomass
Tar

ABSTRACT

Performance of Co–Fe/Al_2O_3 catalysts with the optimum composition (Fe/Co = 0.25) was much higher than corresponding monometallic Co and Fe catalysts in the steam reforming of tar from the pyrolysis of cedar wood in terms of the catalytic activity and the suppression of coke deposition. According to the catalyst characterization, the fcc and bcc Co–Fe alloys were formed by H_2 reduction on the Co–Fe/Al_2O_3 catalyst. In the steam reforming of toluene, the addition of H_2 to the reactant gas enhanced the activity of Co–Fe/Al_2O_3 remarkably. Without H_2 addition, bcc Co–Fe alloy particles were oxidized and this is connected to the deactivation. With H_2 addition, the bcc Co–Fe alloy with an appropriate composition is maintained in metallic state and it contribute to high activity in the steam reforming of toluene.

1. Introduction

Conversion of lignocellulosic biomass to synthesis gas is one of important technologies for the energy utilization of biomass as renewable organic resources [1–4]. This is because synthesis gas is used as a fuel for the gas engine and gas turbine and because it is converted to liquid fuels and chemicals such as hydrocarbons by Fischer–Tropsch synthesis and methanol [1–4]. A most serious problem in the utilization of synthesis gas is the trouble with tar contained in the synthesis gas [3,4]. High reaction temperature has been applied in the non-catalytic gasification in order to decrease the tar amount, however high temperature is unfavorable in terms of the energy efficiency [2]. The conversion of biomass to synthesis gas at lower temperature with higher efficiency has been attempted, and one of effective methods is the utilization of Ni-based catalysts for the gasification and the steam reforming. In particular, the development of the Ni-based catalysts for the gasification of real biomass has been carried out recently, for example, nano-NiO/γ-Al_2O_3 and nano-Ni–La–Fe/Al_2O_3 by Li et al. [5], NiO–MgO solid solution catalyst by Wang et al. [6], Ni loaded brown coal char by Le et al. [7], coal char supported Ni and wood char supported Ni catalysts by Wang et al. [8], NiO-loaded calcined dolomite catalysts by Corujo et al. [9], and so on. In addition, our group has developed modified Ni catalysts supported on Al_2O_3 [10–15] and Ni/Mg/Al nano-composite catalysts [16]. These works have been based on the high activity of Ni metal in the steam reforming of hydrocarbons. On the other hand, supported Co catalysts have been utilized recently for the steam reforming of oxygenates and hydrocarbons such as ethanol [17], methanol [18], naphthalene [19,20], biomass tar [21–23] and wood char [24] and so on, and performance of Co catalysts has been reported to be comparable to that of Ni catalysts [25–28].

In this article, the modification of Co/Al_2O_3 with Fe is attempted. This is because Fe can interact with Co to form Co–Fe alloy, and the synergy between two components with different oxygen affinity is also expected. On the other hand, supported Co catalysts modified with Fe addition have been utilized recently for the steam reforming of oxygenates, such as ethanol [29–33], acetic acid [34] and alcohol [35], and Fischer–Tropsch synthesis [36–40]. In particular, we investigated the performance of Co–Fe/Al_2O_3 catalysts prepared by co-impregnation method in the steam reforming of tar derived from the pyrolysis of cedar. In addition, the performance of the catalysts in the steam reforming of toluene as one of aromatic model compounds of tar was also tested. From the results of these tests and characterization of catalysts before and after the catalytic use, it is found that the bcc Co–Fe alloy particles are important for high catalytic activity.

* Corresponding author. Tel.: +81 22 795 7214; fax: +81 22 795 7214.
E-mail address: tomi@tulip.sannet.ne.jp (K. Tomishige).

0926-3373/$ – see front matter © 2012 Elsevier B.V. All rights reserved.
http://dx.doi.org/10.1016/j.apcatb.2012.03.025

2. Experimental

2.1. Catalyst preparation

The support material of α-Al_2O_3 was prepared by the calcination of γ-Al_2O_3 (KHO-24, Sumitomo Chemical Co., Ltd., 133 $m^2\ g^{-1}$, grain size 2–3 mm) in air at 1423 K. After the calcination, it was crushed and sieved to particle sizes between 0.6 and 2.0 mm. The Co–Fe/Al_2O_3 catalysts were prepared by a co-impregnation method using a mixed aqueous solution of $Co(NO_3)_2{\cdot}6H_2O$ (Wako) and $Fe(NO_3)_3{\cdot}9H_2O$ (Wako). After the impregnation, the samples were dried at 383 K for 12 h followed by the calcination at 773 K for 3 h under air atmosphere. Loading amount of Co on the Co–Fe/Al_2O_3 catalysts was fixed at 12 wt% Co and the loading amount of Fe was in the range of 0.125–1.0 as the molar ratio of Fe to Co (Fe/Co). Monometallic Co/Al_2O_3 and Fe/Al_2O_3 catalysts were also prepared by using the corresponding precursor, and the loading amount of Co and Fe was 12 wt%. The preparation procedure is the same as that of the Co–Fe/Al_2O_3 catalysts.

2.2. Activity test in the steam reforming of tar from the pyrolysis of cedar wood

Cedar wood was ground with a ball mill to about 0.1–0.3 mm size. The moisture content of the cedar wood was 7.2%. The dry-based composition by weight was C 50.8%, H 6.0%, O 41.8%, N 0.2%, and ash 1.1%. The elemental analysis was carried out by the Japan Institute of Energy.

Catalytic performance was evaluated using a laboratory-scale continuous feeding dual-bed reactor that was described in our previous report [11], and the details of the procedure for catalytic performance evaluation in the steam reforming of tar have been also described [11]. The feeding rate of biomass was 60 mg/min, and the feeding rate of C, H, and O was 2360, 3350 and 1450 μmol/min, respectively, excluding the moisture content. The feeding rate of steam was 1110 μmol/min. Here, the molar ratio of feeding steam including biomass moisture to feeding carbon was calculated to be 0.57. The amount of catalyst was 0.75 g or 0.3 g and they were used after the reduction at 773 K with H_2. The formation rate of gaseous products was measured for 15 min, and the rate shown in the results was obtained from the average during 15 min. After the activity test for 15 min, the amount of char and the amount of coke deposited on the catalyst surface were measured by the amount of CO_2 formed by the combustion when the O_2 was fed at 873 K, and the yield of char and coke was calculated by the ratio to the total carbon amount in the fed biomass. As a result, the yields of gaseous products and solid products (coke and char) were determined. The yield of tar is obtained by the subtraction of carbon-based yield of gaseous and solid products from the total. The details are also described in supplementary information.

2.3. Activity test in the steam reforming of toluene

Steam reforming of toluene was conducted in the continuous flow reaction system using a fixed catalyst bed reactor and the procedures and the analysis method were almost the same as reported previously [15]. Catalyst weight was 0.1 g and the catalyst was used after the reduction at 773 K. In this study, we investigated the steam reforming of toluene without or with H_2 addition to the reactant gas. The reaction temperature was 873 K, and the flowing condition was fixed at $W/F = 0.05$ g h/mol, where F represents the total flow rate of toluene, steam, N_2 and H_2. Regarding the used catalysts for the 80 min test, the amount of the deposited coke was also measured by the thermogravimetry (DTA-60, Shimadzu). After the test, a part of the catalyst (ca. 100 mg) was taken out from the inlet and outlet of the catalyst bed. Thermogravimetric analysis (TGA) profiles were obtained under air flowing (50 ml/min) at the heating rate of 10 K/min. Exothermic weight loss was observed at the temperature range between 600 and 900 K. This can be assigned to the combustion of deposited carbon [41]. It is possible to estimate the amount of carbon deposition on the basis of this weight loss. The details are also described in supplementary information.

2.4. Catalyst characterization

The profiles of temperature-programmed reduction (TPR) with H_2 and the amount of H_2 adsorption on the freshly reduced catalysts were obtained in the same method as reported previously [23].

Powder X-ray diffraction (XRD) patterns of the freshly reduced and used catalysts were collected on a Philips X'pert diffractometer using Cu Kα ($\lambda = 0.154$ nm) generated at 40 kV and 20 mA.

Transmission electron microscope (TEM) images and energy dispersive X-ray (EDX) analysis were taken by means of the instrument (JEM-2010F, JEOL) operated at 200 kV. The sample powders after the reduction were dispersed in 2-propanol by supersonic wave and put on Cu grids for TEM observation under air. Average particle size was calculated by $\sum n_i d_i^3 / \sum n_i d_i^2$ (d_i: average particle size, n_i: number of particle with d_i) [42]. The spot size of EDX analysis is ~1 nm.

Co *K*-edge and Fe *K*-edge extended X-ray absorption fine structure (EXAFS) was measured at the BL-9C station of the Photon Factory at the High Energy Accelerator Research Organization in Tsukuba, Japan (Proposal No. 2010G069), and the measurement methods were almost the same as reported previously [23]. The samples for the EXAFS measurement were prepared by pressing the mixture of the catalyst with the same amount of α-Al_2O_3 powder to the disk with 20–25 mg. The thickness of the samples was chosen to be 0.2–0.4 mm (7 mm ϕ) to give edge jump of 0.9–1.6. For the curve fitting analysis, the empirical phase shift and amplitude functions for the Co—Co bond were extracted from the data for Co foil. The curve fitting analysis requires the phase shift and the backscattering amplitude functions. The atomic numbers of Co and Fe are similar; therefore, the phase shift and the amplitude functions are almost the same. The structure of Co metal is fcc and it is easy to extract the phase shift and the amplitude functions of the Co—Co bond from Co metal. On the other hand, the structure of Fe metal is bcc and it is not easy to extract them because the distance of first and second-nearest Fe—Fe bonds is close. In the case of Co and Fe *K*-edge EXAFS of Co–Fe/Al_2O_3 catalysts, there can be Co—Co, Co—Fe, Fe—Fe and Fe—Co bonds. For the reason mentioned above, the phase shift and amplitude functions extracted from Co metal for the Co—Co bond were applied to the Co—Fe, Fe—Fe and Fe—Co bonds. In the curve fitting analysis of Co and Fe *K*-edge EXAFS, the absorbing and backscattering atoms were represented as Co—Co (or —Fe) and Fe—Co (or —Fe) bonds, respectively, on Co—Fe/Al_2O_3 (Fe/Co = 0.25), because the amount of Co was much larger than that of Fe. The details are also described in supplementary information.

3. Results and discussion

3.1. Catalytic performance of Co–Fe/Al_2O_3 in the steam reforming of tar

Fig. 1 shows the catalytic performance of Co–Fe/Al_2O_3, Co/Al_2O_3 and Fe/Al_2O_3 in steam reforming of tar at 823 K. In the case of Fe/Al_2O_3, the amount of the residual tar was large and the ratio of H_2 to CO (H_2/CO) was rather low, indicating the low reforming activity of Fe/Al_2O_3. The addition of Fe to Co/Al_2O_3 decreased the amount of tar in the range of the molar ratio of Fe to Co (Fe/Co) ≤ 0.25, and this means that Fe addition promoted the steam reforming of tar. When the 0.75 g catalyst was used, almost all of tar was

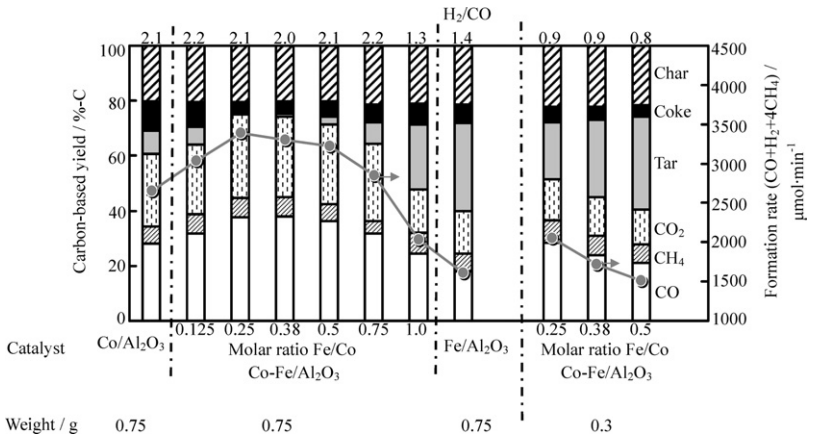

Fig. 1. Catalytic performance in steam reforming of tar over Co–Fe/Al_2O_3 catalysts at 823 K.

converted over the catalysts with Fe/Co = 0.25, 0.38 and 0.5. In order to optimize the Fe amount more precisely, the catalysts were also tested with 0.3 g of catalysts (Fe/Co = 0.25, 0.38, 0.5). As a result, it is concluded that Co–Fe/Al_2O_3 (Fe/Co = 0.25) was optimum, and the addition of Fe at the optimum amount enhanced the reforming activity and decreased the coke amount. The excess addition of Fe (Fe/Co > 0.5) decreased the catalytic performance significantly. This behavior is similar to the dependence of the additive amount of Fe over Ni–Fe/Al_2O_3 on the catalytic performance in the steam reforming of tar in the previous report [43], although the optimum amount of Fe on Co/Al_2O_3 was different from that on Ni/Al_2O_3 (Fe/Ni = 0.5).

Fig. 2 shows the reaction temperature dependence of the catalytic performance in the steam reforming of tar over Co–Fe/Al_2O_3 (Fe/Co = 0.25), Co/Al_2O_3 and Fe/Al_2O_3. The Fe/Al_2O_3 catalyst showed low reforming activity even at 923 K, and much higher reaction temperature was needed for the total removal of the residual tar. The Co/Al_2O_3 showed much higher reforming activity and the tar yield became almost zero at 873 K and 923 K. In the case of Co–Fe/Al_2O_3 (Fe/Co = 0.25), the tar yield was almost zero even at 823 K, indicating higher reforming activity of Co–Fe/Al_2O_3 than that of Co/Al_2O_3. The performance of Co–Fe/Al_2O_3 (Fe/Co = 0.25) at 823 K was comparable to that of Co/Al_2O_3 at 873 K, suggesting that the reaction temperature can be decreased by the catalyst with high performance. Another important point is that the addition of Fe can suppress the coke deposition.

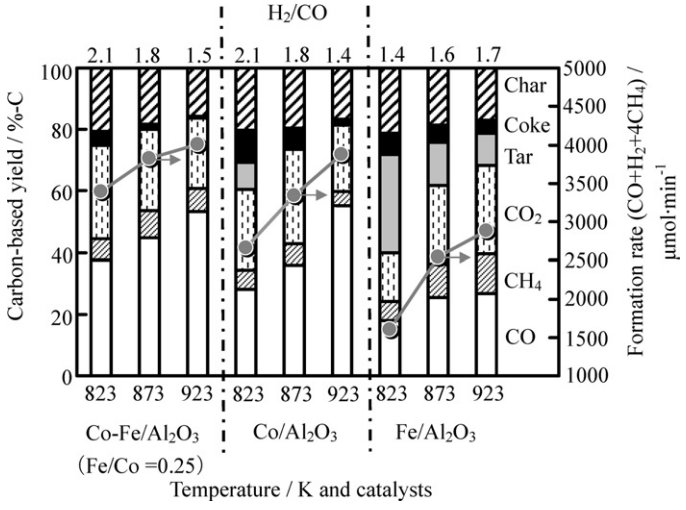

Fig. 2. Reaction temperature dependence in steam reforming of tar over Fe/Al_2O_3, Co/Al_2O_3 and Co–Fe/Al_2O_3 (Fe/Co = 0.25) after H_2 reduction. Catalyst weight was 0.75 g.

Fig. 3 shows the formation rate of gaseous products as a function of time on stream over Co–Fe/Al_2O_3 (Fe/Co = 0.25) at 873 K. According to our previous report, Co(12 wt%)/Al_2O_3 is deactivated after 40 min under the same reaction conditions[23]. On the other hand, Co–Fe/Al_2O_3 (Fe/Co = 0.25) maintained the activity for 60 min, and Co–Fe/Al_2O_3 (Co/Ni = 0.25) was more stable than Co(12 wt%)/Al_2O_3. One possible explanation of high stability of Co–Fe/Al_2O_3 (Fe/Co = 0.25) is due to the higher resistance to coke formation.

3.2. Catalyst characterization of fresh catalysts

Fig. 4 shows the TPR profiles of Co–Fe/Al_2O_3 with various Fe amounts, Fe/Al_2O_3 and Co/Al_2O_3. The reduction of Fe species on Fe/Al_2O_3 proceeded in wide temperature range of 573–1173 K, on the other hand, the reduction of Co species on Co/Al_2O_3 proceeded in narrow temperature range of 473–773 K. These results indicate that the Co species has higher reducibility than Fe species on Al_2O_3. In the case of Co–Fe/Al_2O_3, the H_2 consumption peaks are located between those of Co/Al_2O_3 and Fe/Al_2O_3, and the temperature range was 573–873 K. The absence of H_2 consumption peak above 873 K on Co–Fe/Al_2O_3 indicates that the reduction of Fe is promoted remarkably by the presence of Co. At the same time, the peak top of the H_2 consumption on Co–Fe/Al_2O_3 was shifted to higher temperature than that on Co/Al_2O_3, indicating that the reduction of Co is suppressed slightly by the presence of Fe. The amount of H_2 consumption below 873 K is listed in Table 1 and is discussed later.

Fig. 5 shows the XRD patterns of Fe/Al_2O_3, Co/Al_2O_3 and Co–Fe/Al_2O_3 after the calcination before the reduction pretreatment. The peak intensity was normalized by the peak assigned

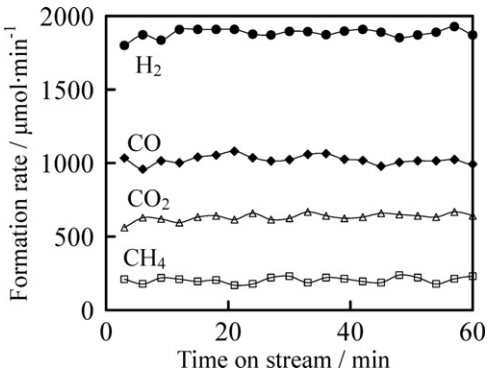

Fig. 3. Reaction time dependence in steam reforming of tar at 873 K over Co–Fe/Al_2O_3 (Fe/Co = 0.25). Catalyst weight was 0.75 g.

Table 1
Properties of the catalysts after H_2 reduction at 773 K.

Catalyst	Fe/Co	Content (mmol g^{-1}-cat)		H_2 consumption[a] in TPR (mmol g^{-1}-cat)	H_2 consumption[b] (mmol g^{-1}-cat) (3/2Fe) + (4/3Co)	H_2 adsorption (10^{-6} mol g^{-1}-cat)	Dispersion/% H/(Co + Fe)[d]
		Co	Fe				
Co/Al_2O_3	0	2.0	–	2.7	2.67	30	3.0
$Co–Fe/Al_2O_3$	0.13	2.0	0.26	2.9	3.06	50	4.4
	0.25	2.0	0.50	3.2	3.42	47	3.8
	0.38	2.0	0.75	3.6	3.79	44	3.2
	0.50	2.0	1.0	3.7	4.17	34	2.3
	0.75	2.0	1.5	4.6	4.92	34	1.9
	1.0	2.0	2.0	5.4	5.67	32	1.6
Fe/Al_2O_3	–	–	2.0	1.2/(3.2)[c]	3.15	0.3	–

[a] H_2 consumption below 873 K in TPR profiles shown in Fig. 4.
[b] The stoichiometry assumed is: $Fe_2O_3 + 3H_2 \rightarrow 2Fe + 3H_2O$ and $Co_3O_4 + 4H_2 \rightarrow 3Co + 4H_2O$.
[c] H_2 consumption below 1273 K in TPR profiles shown in Fig. 4.
[d] Dispersion of metal particles: $2 \times (H_2$ adsorption amount$)/(Co + Fe) \times 100\%$.

to α-Al_2O_3 at $2\theta = 43.4^\circ$ and the content of α-Al_2O_3. The peak due to Co_3O_4 was observed at $2\theta = 36.84^\circ$ on Co/Al_2O_3 [44], and the peak due to Fe_2O_3 was observed at $2\theta = 33.24^\circ$ and 35.72° on Fe/Al_2O_3 [45]. In the case of $Co–Fe/Al_2O_3$ (Fe/Co = 0.13, 0.25), the peak assigned to Co_3O_4 was observed and the peaks assigned to Fe_2O_3 were not observed. The peak assigned to Co_3O_4 was shifted to smaller angle gradually with increasing Fe content, suggesting the formation of Co_3O_4–Fe_3O_4 mixed oxide. Considering that the peak position due to Fe_3O_4 and $CoFe_2O_4$ is $2\theta = 35.43^\circ$ and 35.44°, respectively [46,47], the peak shift was relatively small, and this indicates the formation of Co_3O_4–Fe_3O_4 mixed oxide with very low Fe content. On the other hand, at Fe/Co $\geq$ 0.38, the peaks assigned to Fe_2O_3 appeared, and the peak position was shifted to smaller angle and it approached the position of Fe_2O_3 on Fe/Al_2O_3 gradually when the added Fe amount was increased, suggesting the formation of Fe_2O_3–Co_2O_3 mixed oxide. Since the peak shift from Fe_2O_3 was very small like the case of Co_3O_4–Fe_3O_4, the Co content in the Fe_2O_3–Co_2O_3 mixed oxide can be also very low. The intensity of the peak around $2\theta = 36.8^\circ$ on $Co–Fe/Al_2O_3$ with various Fe contents was almost comparable to that of Co/Al_2O_3, and this also supports that the Fe content in the Co_3O_4–Fe_3O_4 phase is rather small. At the same time, the intensity of the peak around $2\theta = 33.2^\circ$ of $Co–Fe/Al_2O_3$ (Fe/Co = 1) was almost comparable to that of Fe/Al_2O_3, and this also supports that the Co content in the Fe_2O_3–Co_2O_3 phase is also rather small. Based on the XRD results of the fresh catalysts, the Co and Fe species on $Co–Fe/Al_2O_3$ are mainly due to Co_3O_4 and Fe_2O_3. Therefore, the H_2 consumption in the TPR is calculated from the reduction of Co_3O_4 and Fe_2O_3, and the calculated results are listed in Table 1. The H_2 consumption in the TPR below 873 K based on Fig. 4 on $Co–Fe/Al_2O_3$ was slightly smaller than that calculated. This is probably due to the mixed oxide formation, for example, Fe^{2+} in the Co_3O_4–Fe_3O_4 mixed oxide. The H_2 consumption of Fe/Al_2O_3 below 1273 K is comparable to that estimated from the stoichiometry (Table 1), and this TPR result suggests the absence of the unreduced Fe.

Fig. 6 shows the XRD patterns of Fe/Al_2O_3, Co/Al_2O_3 and $Co–Fe/Al_2O_3$ after the H_2 reduction at 773 K for 0.5 h. The TPR results indicated that most Co and Fe species are reduced by the reduction pretreatment on Co/Al_2O_3 and $Co–Fe/Al_2O_3$ catalysts. The peak due to Fe metal with bcc structure was observed at

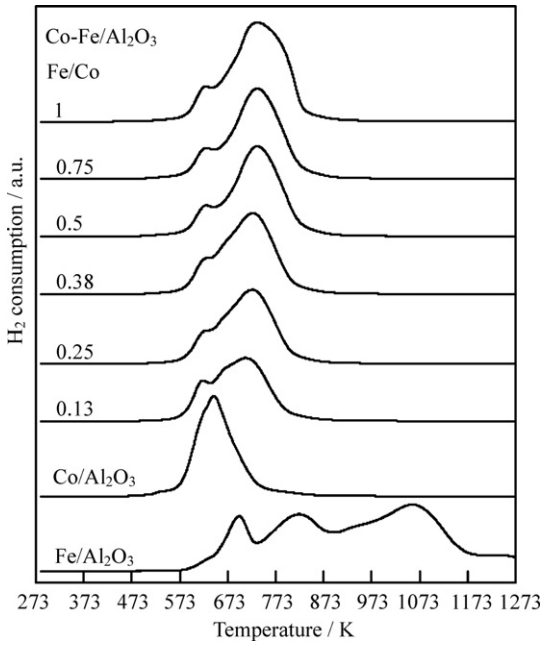

Fig. 4. TPR profiles of Fe/Al_2O_3, Co/Al_2O_3 and $Co–Fe/Al_2O_3$ catalysts. TPR conditions: heating rate 10 K/min, 5% H_2/Ar flow rate 30 ml/min. Sample weight: 50 mg.

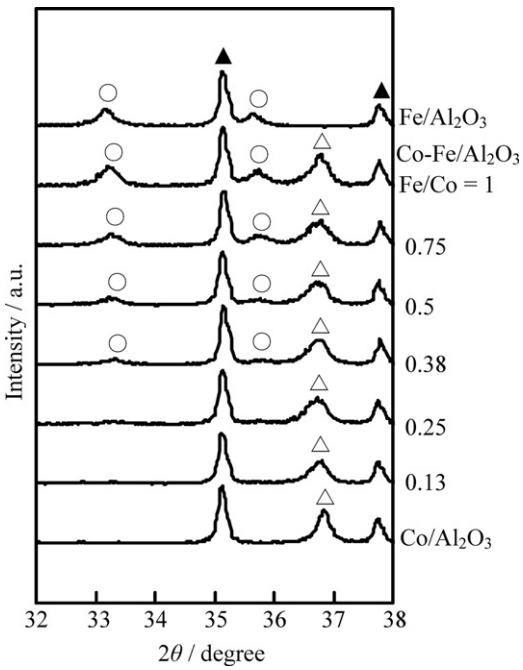

Fig. 5. XRD patterns of the calcined catalysts. △ = Co_3O_4 or Co_3O_4–Fe_3O_4 mixed oxides with low Fe content, ○ = Fe_2O_3 or Fe_2O_3–Co_2O_3 mixed oxides with very low Co content, ▲ = Al_2O_3.

Table 2
Composition of fcc and bcc Co–Fe alloy phase on Co–Fe/Al_2O_3 and the distribution of Co and Fe in each alloy.

Catalyst	M (Fe/Co)	Experimental [a]		Calculated Fe/(Co + Fe)		Calculated Fe/Co		Distribution	
		$d_{fcc\ Co-Fe}$ (nm)	$d_{bcc\ Co-Fe}$ (nm)	fcc Co–Fe	bcc Co–Fe	fcc Co–Fe	bcc Co–Fe	$Co_{bcc\ Co-Fe}/(Co_{fcc\ Co-Fe} + Co_{bcc\ Co-Fe})$	$Fe_{bcc\ Co-Fe}/(Fe_{fcc\ Co-Fe} + Fe_{bcc\ Co-Fe})$
Co–Fe/Al_2O_3	0.13	0.2046	0.2009	0.06	0.35	0.06	0.35	0.24	0.65
	0.25	0.2047	0.2009	0.08	0.35	0.09	0.44	0.46	0.80
	0.38	0.2048	0.2009	0.10	0.38	0.11	0.55	0.61	0.89
	0.5	0.2048	0.2010	0.10	0.42	0.11	0.67	0.70	0.94
	0.75	–	0.2012	–	0.46	–	0.75	1.00	1.00
	1.0	–	0.2013	–	0.51	–	1.00	1.00	1.00
	0.25[b]	0.2052	–	0.16	–	0.18	–	–	–
	0.25[c]	0.2050	0.2013	0.13	0.51	0.14	0.58	–	–
	0.25[d]	0.2048	0.2006	0.10	0.26	0.11	0.31	–	–

[a] Fig. 6.
[b] Fig. 10(b): after steam reforming of toluene without hydrogen for 80 min (Fig. 9(a)).
[c] Fig. 10(c): after steam reforming of toluene with hydrogen for 80 min (Fig. 9(b)).
[d] Fig. 10(d): after steam reforming of tar for 60 min (Fig. 3).

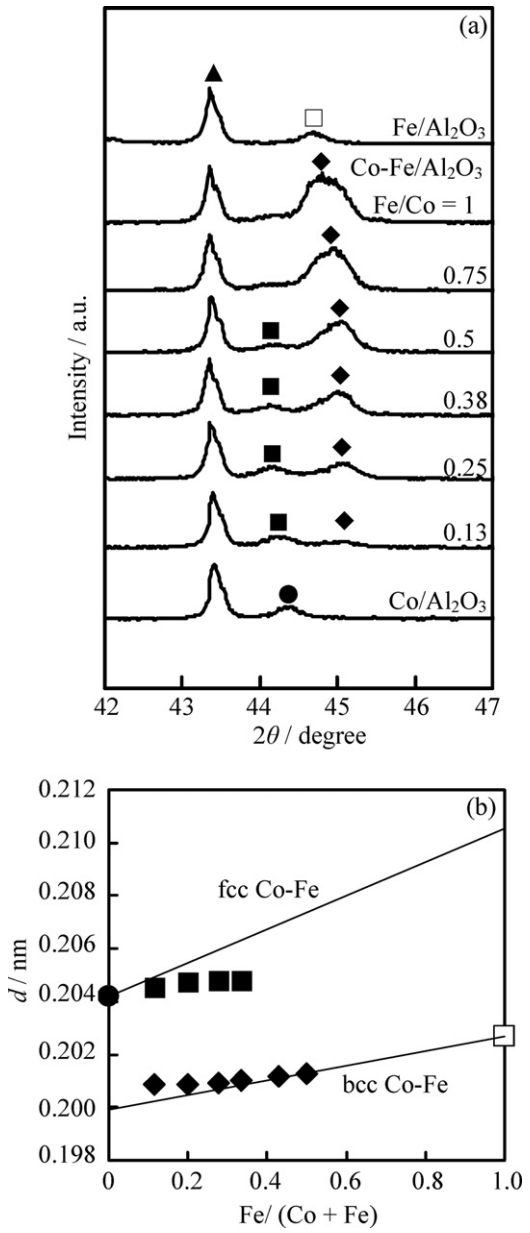

Fig. 6. (a) XRD patterns of the reduced catalysts, and (b) d spacing of the peaks of Co, Fe, fcc Co–Fe and bcc Co–Fe as a function of Fe/(Co + Fe). ● = Co, □ = Fe, ■ = fcc Co–Fe solid solution alloy, ♦ = bcc Co–Fe solid solution alloy, and ▲ = Al_2O_3.

$2\theta = 44.7^\circ$ on Fe/Al_2O_3 [48], and the peak due to Co metal with fcc structure was observed at $2\theta = 44.28^\circ$ on Co/Al_2O_3 [49]. In the case of Co–Fe/Al_2O_3 (Fe/Co = 0.13–0.5), the two peaks in the range of $2\theta = 44.0$–45.3° were observed. The peak around $2\theta = 44.1^\circ$ was shifted to smaller angle gradually with increasing Fe amount, on the other hand, the intensity of the peak decreased with increasing Fe amount, and it is difficult to recognize the peak and its position on Co–Fe/Al_2O_3 (Fe/Co = 0.75 and 1). According to the previous reports, the peak is interpreted by the formation of Co–Fe solid solution alloy with fcc structure [37,50,51]. The peak position around $2\theta = 45.1^\circ$ was shifted to smaller angle with increasing the Fe content approaching that due to Fe metal with bcc structure, and this peak is assigned to the formation of Co–Fe solid solution alloy with bcc structure on the basis of the previous reports [50,52–54]. An important point is that the intensity of the peak due to bcc Co–Fe alloy increased with increasing the added Fe content. Fig. 6(b) shows the d spacing of fcc and bcc Co–Fe alloy phases as a function of the composition (Fe/(Co + Fe)) on Co/Al_2O_3, Fe/Al_2O_3 and Co–Fe/Al_2O_3 catalysts. It has been known that the lattice constant of the solid solution alloy is given from a linear combination of the lattice constant of each component, according to Vegard's law [55]. In order to apply this Vegard's law to the results of these catalysts, the d-spacings of bcc and fcc Co–Fe alloy were calculated using the lattice constant of bcc Co metal 0.2827 nm [56] and fcc Fe metal 0.3646 nm [57], and these are also shown as lines in Fig. 6(b). The d spacings obtained from the XRD results are also plotted in Fig. 6(b). From the comparison between the line of Vegard's law and the d spacings obtained from the experimental results in Fig. 6(a), it is possible to estimate the actual composition in the fcc and bcc Co–Fe alloys assuming the homogeneous composition of each phase. Table 2 lists the obtained composition of fcc and bcc Co–Fe alloy phases. The obtained molar ratio of Fe/Co in fcc Co–Fe alloy phase was smaller than the average molar ratio, indicating the formation of bcc Co–Fe alloy with higher Fe content than the average ratio. Even when the molar ratio of Fe/Co in bcc Co–Fe alloy is much smaller than 1, the bcc Co–Fe alloy was formed, indicating that the alloying of Co with relatively small amount of Fe can transform the fcc structure to the bcc structure. In addition, it should be noted that the distribution of Co and Fe in the fcc and bcc Co–Fe alloys can be calculated and also listed in Table 2. The distribution of Co to bcc Co–Fe alloy increased with increasing the average molar ratio of Fe to Co, and the distribution of Fe to bcc Co–Fe alloy is high and Fe atoms tend to be present in bcc Co–Fe alloy mainly.

Fig. 7 shows the TEM images of the Co/Al_2O_3 and Co–Fe/Al_2O_3 (Fe/Co = 0.25) after H_2 reduction at 773 K. The average size of metallic particles of Co/Al_2O_3 and Co–Fe/Al_2O_3 (Fe/Co = 0.25) was estimated to be 29 ± 3 and 28 ± 3 nm, respectively. The elemental composition of the various positions on the Co–Fe/Al_2O_3 (Fe/Co = 0.25) was measured by the EDX analysis as listed in Table 3.

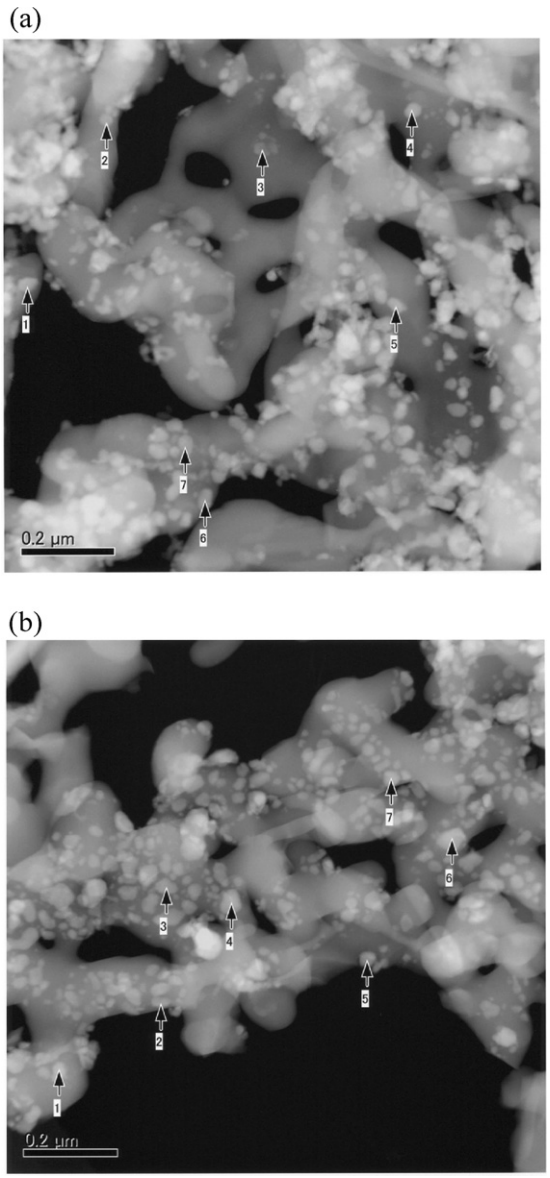

Fig. 7. TEM images of the Co–Fe/Al_2O_3 (Fe/Co = 0.25) (a) and Co/Al_2O_3 (b) after H_2 pretreatment at 773 K. The numbers in the image indicate the position of the EDX analysis.

The molar ratio of Fe/Co obtained from the EDX analysis was in the range of 0.09–0.20, which are not far from the average composition (Fe/Co = 0.25). At present, it does not seem to be possible to determine the composition of fcc Co–Fe and bcc Co–Fe alloys, separately.

Table 3
Results of energy-dispersive X-ray analysis of the Co–Fe/Al_2O_3 (Fe/Co = 0.25) after the H_2 reduction at 773 K.

Position in Fig. 7(a)	Molar ratio		
	Co	Fe	Fe/Co
1	0.88	0.13	0.14
2	0.83	0.17	0.20
3	0.89	0.11	0.13
4	0.92	0.08	0.09
5	0.82	0.14	0.17
6	0.86	0.14	0.17
7	0.86	0.14	0.17

The amount of H_2 adsorption on the fresh catalysts after the reduction at 773 K is also listed in Table 1. The amount of H_2 adsorption on Co/Al_2O_3 gave the dispersion of 3.0%. The peak width in the XRD pattern of the reduced Co/Al_2O_3 gave 32 ± 3 nm metal particle size (d) [58], where the dispersion (D %) is calculated to be 3.0% using the equation ($d = 9.61/D$) [59]. The particle size from TEM (29 nm) gives the dispersion of 3.0%. The dispersion given from these methods agreed with each other. The addition of Fe in the range of Fe/Co = 0.13–0.38 increased the H_2 adsorption amount, and excess Fe addition decreased the H_2 adsorption. This tendency agreed well with the performance in the steam reforming of tar, and the promoting effect of Fe addition is explained by the increase of H_2 adsorption amount. On the other hand, the particle size on Co–Fe/Al_2O_3 (Fe/Co = 0.25) determined by TEM (28 nm) was almost the same as that of Co/Al_2O_3 (29 nm). Therefore, the increase of H_2 adsorption amount cannot be caused by the decrease of metal particles size. The amount of H_2 adsorption on Co–Fe/Al_2O_3 (Fe/Co = 0.25) was high for the particle size. This may be due to the formation of bcc Co–Fe alloy, and further investigation is necessary for the elucidation of the mechanism.

In order to analyze the local structure around Co and Fe atoms, the catalysts were characterized by Co *K*-edge and Fe *K*-edge EXAFS. Fig. 8 shows EXAFS results of Co/Al_2O_3, Co–Fe/Al_2O_3 (Fe/Co = 0.25) and reference compounds. The curve fitting results are listed in Tables 4 and 5. In the EXAFS analysis of Co/Al_2O_3, the coordination number (CN) of the Co—Co bond was 11.2, which is close to the CN of the Co—Co bond in Co foil (CN = 12). This is explained by the low dispersion of Co metal particles on Co/Al_2O_3 as mentioned above. In the case of Co *K*-edge EXAFS of Co–Fe/Al_2O_3 (Fe/Co = 0.25) after the reduction, two different Co—Co (or Fe) bonds were applied to the curve fitting analysis judging from the XRD results indicating the presence of fcc and bcc Co–Fe alloy. According to the XRD analysis, the ratio of Co in the bcc Co–Fe alloy to the total Co is estimated to be 0.46, and that in the fcc Co–Fe alloy is estimated to be 0.54. Based on this distribution of Co, the bulk CN of the nearest bond is 10.2 ($=0.54 \times 12 + 0.46 \times 8$) and that of the second-nearest bond is 2.8 ($=0.46 \times 6$). The curve fitting analysis gave the slightly lower CNs (9.6 and 2.4) than the bulk ones, and these behaviors are explained by low dispersion of Co–Fe alloy particles. These CNs were decreased by the passivation (8.1 and 1.6), and this is interpreted by the breaking of Co—Co (or Fe) bond with the oxidation. Table 5 lists the curve fitting results of Fe *K*-edge EXAFS of Fe foil and Co–Fe/Al_2O_3 (Fe/Co = 0.25) catalyst. The curve fitting analysis of Fe foil was carried out in order to check the validity of the phase shift and the backscattering amplitude functions extracted from Co foil. In the case of Co–Fe/Al_2O_3 after the reduction, the ratio of Fe in the bcc Co–Fe alloy to the total Fe is estimated to be 0.80, and that in the fcc Co–Fe alloy is estimated to be 0.20 on the basis of the XRD results (Table 3). Therefore, the bulk CNs of the nearest bond is 8.8 ($=0.20 \times 12 + 0.80 \times 8$) and that of the second-nearest bond is 4.8 ($=0.80 \times 6$). The curve fitting analysis also gave slightly lower CNs (7.4 and 3.8) than the bulk ones, and this corresponds to the low dispersion of Co–Fe alloys. An important point is that the passivation treatment did not decrease the CNs (7.3 and 3.5) of Fe *K*-edge EXAFS so significantly, and this behavior in the Fe *K*-edge EXAFS analysis is different from that in the Co *K*-edge EXAFS analysis. This suggests that the oxidation of Co is more preferable than that of Fe on Co–Fe/Al_2O_3 (Fe/Co = 0.25). The oxygen affinity of Fe is usually higher than that of Co [60], and this cannot explain the present oxidation behavior. One possible interpretation is the surface segregation of Co on the Co–Fe alloys.

3.3. Catalytic performance in the steam reforming of toluene

It has been known that toluene is one of the typical components in the tar from the biomass pyrolysis, and the reactivity

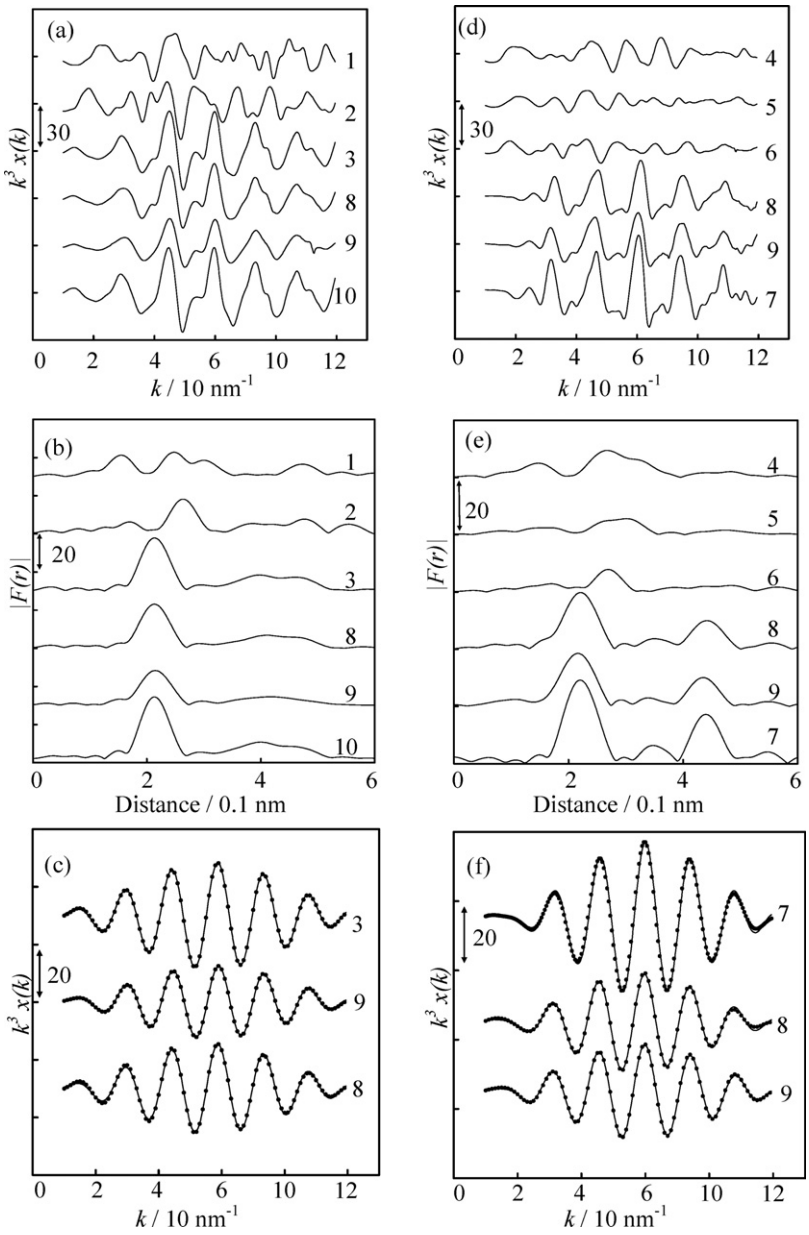

Fig. 8. Results of EXAFS analysis of Co–Fe/Al_2O_3 (Fe/Co = 0.25) and Co/Al_2O_3. 1. Co_3O_4, 2. CoO, 3. Co/Al_2O_3 after the reduction at 773 K, 4. Fe_2O_3, 5. Fe_3O_4, 6. FeO, 7. Fe foil, 8. Co–Fe/Al_2O_3 (Fe/Co = 0.25) after the reduction at 773 K, 9. Co–Fe/Al_2O_3 (Fe/Co = 0.25) after the reduction and passivation at r.t., and 10. Co foil. (a–c) Co *K*-edge, (d–f) Fe *K*-edge, and (a and d) k^3-weighted EXAFS oscillation. (b and e) Fourier transform of k^3-weighted EXAFS, FT range: 30–120 nm^{-1}. (c and f) Fourier filtered EXAFS data (solid line) and calculated data (dotted line), Fourier filtering range: 0.1626–0.2700 nm for Co *K*-edge, 0.1626–0.2823 nm for Fe *K*-edge.

of aromatic hydrocarbons can be evaluated from the results of the toluene steam reforming [15,61,62]. Table 6 lists the results of the activity test in the steam reforming of toluene with and without adding the external hydrogen at the reaction time of 30 min. Here, the contact time was adjusted to the conditions where the conversion is far from 100% for the comparison in terms of the catalytic activity. It is clear that the activity order without hydrogen addition is as follows: Co/Al_2O_3 > Co–Fe/Al_2O_3

Table 4
Curve fitting results of Co *K*-edge EXAFS of Co/Al_2O_3 and Co–Fe/Al_2O_3 (Fe/Co = 0.25) catalysts.

Catalyst	Pretreatment	Shells	CN[a]	R (10^{-1} nm)[b]	σ (10^{-1} nm)[c]	ΔE_0 (eV)[d]	R_f (%)[e]
Co/Al_2O_3	Reduction	Co—Co	11.2	2.51	0.065	0.64	0.2
Co–Fe/Al_2O_3 (Fe/Co = 0.25)	Reduction	Co—Co (or Fe)	9.6	2.49	0.072	−3.3	0.2
		Co—Co (or Fe)	2.4	2.86	0.065	−4.2	
	Reduction + passivation	Co—Fe (or Co)	8.1	2.50	0.072	−0.77	0.1
		Co—Fe (or Co)	1.6	2.89	0.065	−2.5	

[a] Coordination number.
[b] Bond distance.
[c] Debye–Waller factor.
[d] Difference in the origin of photoelectron energy between the reference and the sample.
[e] Residual factor. Fourier filtering range: 0.1626–0.2700 nm.

Table 5
Curve fitting results of Fe *K*-edge EXAFS of Fe foil and Co–Fe/Al_2O_3 (Fe/Co = 0.25) catalyst.

Catalyst	Pretreatment	Shells	CN[a]	R (10^{-1} nm)[b]	σ (10^{-1} nm)[c]	ΔE_0 (eV)[d]	R_f (%)[e]
Fe foil	Reduction	Fe—Fe	8	2.48	0.06	0.99	0.7
		Fe—Fe	6	2.86	0.06	−0.69	
Co–Fe/Al_2O_3[f]	Reduction	Fe—Co (or Fe)	7.4	2.48	0.072	−0.55	0.3
		Fe—Co (or Fe)	3.8	2.86	0.071	−0.96	
	Reduction + passivation	Fe—Co (or Fe)	7.3	2.48	0.072	−1.1	0.2
		Fe—Co (or Fe)	3.5	2.86	0.071	−2.9	

[a] Coordination number.
[b] Bond distance.
[c] Debye–Waller factor.
[d] Difference in the origin of photoelectron energy between the reference and the sample.
[e] Residual factor. Fourier filtering range: 0.1626–0.2823 nm.

Table 6
Catalytic performance in the steam reforming of toluene.

Flow condition (mmol min^{-1})				Catalyst	Toluene conv. (%)	Formation rate (μmol/min)				H_2/CO
Toluene	H_2O	N_2	H_2			CO	CO_2	Benzene	H_2	
0.38	4.4	26.8	0.0	Co/Al_2O_3	55.3	438	999	2	3240	7.4
				Co–Fe/Al_2O_3 (Fe/Co = 0.25)	15.8	86	316	2	944	11.0
				Co–Fe/Al_2O_3 (Fe/Co = 0.5)	9.5	35	204	2	577	16.5
0.38	4.4	23.0	3.8	Co/Al_2O_3	39.0	450	553	3	2109	4.7
				Co–Fe/Al_2O_3 (Fe/Co = 0.25)	62.7	717	838	16	3289	4.6
				Co–Fe/Al_2O_3 (Fe/Co = 0.5)	21.1	205	307	7	1114	5.4
0.38	4.4	19.2	7.6	Co/Al_2O_3	33.1	457	380	3	1666	3.6
				Co–Fe/Al_2O_3 (Fe/Co = 0.25)	71.3	983	752	24	3487	3.5
				Co–Fe/Al_2O_3 (Fe/Co = 0.5)	49.7	578	579	25	2408	4.2

Reaction condition: W = 100 mg, W/F = 0.05 g h/mol, reaction temperature 873 K, reaction time 30 min.

(Fe/Co = 0.25) > Co–Fe/Al_2O_3 (Fe/Co = 0.5). The effect of H_2 addition to the reactant gas was strongly dependent on the catalysts. The toluene conversion on Co/Al_2O_3 decreased gradually with increasing partial pressure of hydrogen (55.3 → 39.0 → 33.1), on the other hand, the toluene conversion on both Co–Fe/Al_2O_3 catalysts increased remarkably with increasing the partial pressure of hydrogen in the reactant gas (15.8 → 62.7 → 71.3). When the hydrogen partial pressure was highest, the activity order was as follows: Co–Fe/Al_2O_3 (Fe/Co = 0.25) > Co–Fe/Al_2O_3 (Fe/Co = 0.5) > Co/Al_2O_3. This activity order gave similar tendency in the steam reforming of tar (Fig. 1).

Fig. 9 shows the formation rate of the products and toluene conversion as a function of time on stream over Co–Fe/Al_2O_3 (Fe/Co = 0.25). In the absence of H_2 addition, the activity decreased significantly with increasing reaction time. Although the details are not shown, Co/Al_2O_3 showed stable activity in the steam reforming of toluene without hydrogen addition. Under this condition, Co/Al_2O_3 gave 55.3% toluene conversion as listed in Table 6. On the other hand, the toluene conversion at the initial stage on Co–Fe/Al_2O_3 (Fe/Co = 0.25) was beyond 60% and it is also expected that the conversion was much higher than 60% considering from the conversion decrease during the initial 5 min. Judging from this reaction time dependence, it is found that Co–Fe/Al_2O_3 (Fe/Co = 0.25) has high catalytic activity in the steam reforming of toluene, and the deactivation rate is high. The stability of Co–Fe/Al_2O_3 (Fe/Co = 0.25) was improved by the hydrogen addition (Fig. 9(b)). After this stability test, we measured the amount of deposited carbon using the TGA apparatus, because the carbon deposition may cause the catalyst deactivation [63–69]. The amount of the deposited carbon on Co–Fe/Al_2O_3 (Fe/Co = 0.25) after the 80 min reaction in the toluene steam reforming in the absence and presence of H_2 addition was determined to be 5 and 15 mg g^{-1}-cat, and this tendency cannot explain the deactivation of Co–Fe/Al_2O_3 (Fe/Co = 0.25) in the absence of H_2 addition at all.

3.4. Catalyst characterization after the catalytic use

Fig. 10 shows the XRD patterns of Co–Fe/Al_2O_3 (Fe/Co = 0.25) after the 80 min reaction of toluene steam reforming without and with H_2 addition. After the reduction, both fcc and bcc Co–Fe alloys were detected, however, after the reaction without H_2 addition, the peak due to bcc Co–Fe alloy disappeared. This suggests that fcc Co–Fe is not oxidized and bcc Co–Fe is oxidized during the reaction. The results of the XRD analysis after the reaction are also summarized in Table 2. After the steam reforming of toluene without hydrogen addition, the obtained Fe/Co (0.18) in the fcc Co–Fe alloy became a little higher than that after the reduction (0.11). The increase of Fe/Co in the fcc Co–Fe alloy may be explained by the phase transition from the bcc Co–Fe alloy with higher Fe/Co to the fcc Co–Fe alloy with the oxidation. Preferential oxidation of Fe in the bcc Co–Fe alloy can decrease the Fe/Co in the reduced phase and promote the phase transition to fcc Co–Fe alloy which is more stable at lower Fe/Co. On the other hand, after the steam reforming of toluene with hydrogen addition, the Fe/Co was increased by the steam reforming of toluene in both fcc and bcc Co–Fe alloys. As suggested by the EXAFS analysis, the oxidation of Co is more preferable than that of Fe by passivation of the surface of metal particles. When Co is preferentially oxidized, the Fe/Co ratio in the alloys can be increased. The oxidation rate of the bcc Co–Fe alloy phase can be much higher than that of fcc Co–Fe alloy phase judging from the XRD results. As mentioned above, the Fe/Co ratio in the bcc Co–Fe alloy phase was higher than that in the fcc Co–Fe alloy phase (Table 2). Considering higher oxygen affinity of Fe than Co [60], the bcc Co–Fe alloy phase has lower resistance to the oxidation. Fig. 10(d) shows the XRD pattern of Co–Fe/Al_2O_3 (Fe/Co = 0.25) after the reaction of the steam reforming of tar for 60 min. The peak due to fcc Co–Fe alloy was maintained and the peak due to bcc Co–Fe alloy became weak and it was shifted slightly to the larger angle. These XRD results are also summarized in Table 2. Calculated Fe/Co

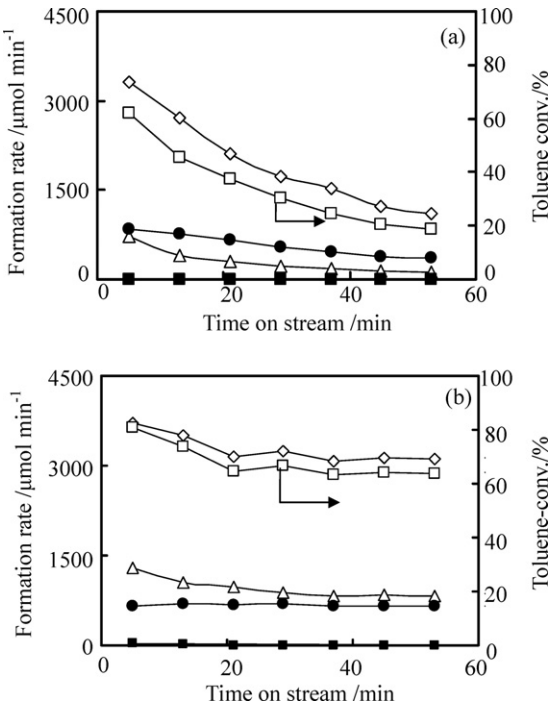

Fig. 9. Reaction time dependence of the formation rates of products and toluene conversion in steam reforming of toluene without (a) or with (b) hydrogen addition to the reactant gas over Co–Fe/Al_2O_3 (Fe/Co = 0.25) at 873 K. □: toluene conversion, △:CO, ●:CO_2, ■:CH_4, ◇: H_2. Feeding rate: (a) toluene 0.38 mmol min^{-1}, steam 4.4 mmol min^{-1}, N_2 26.8 mmol min^{-1}. (b) Toluene 0.38 mmol min^{-1}, steam 4.4 mmol min^{-1}, N_2 19.2 mmol min^{-1}, H_2 7.6 mmol min^{-1}, W = 100 mg, W/F = 0.05 g h/mol.

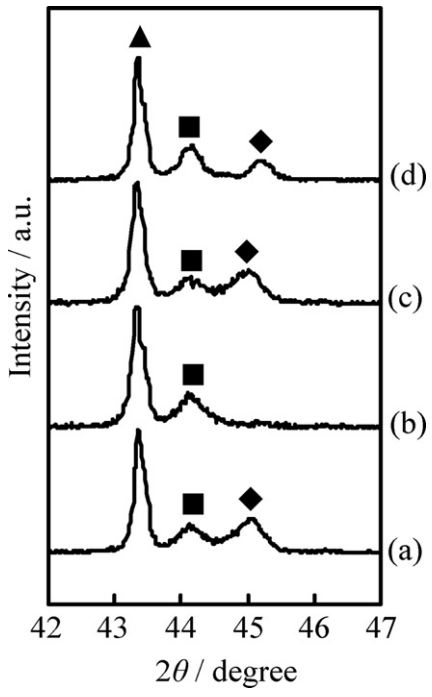

Fig. 10. XRD patterns of Co–Fe/Al_2O_3 (Fe/Co = 0.25) after various treatments. (a) After the reduction pretreatment, (b) after steam reforming of toluene without hydrogen for 80 min (Fig. 9(a)), (c) after steam reforming of toluene with hydrogen for 80 min (Fig. 9(b)), (d) after steam reforming of tar at 873 K for 60 min (Fig. 3). ■ = fcc Co–Fe solid solution alloy, ♦ = bcc Co–Fe solid solution alloy, ▲ = α-Al_2O_3.

in the fcc Co–Fe alloy was increased very slightly, however, that in the bcc Co–Fe alloy was decreased significantly. The composition (Fe/Co) in the bcc Co–Fe alloy decrease during the tar steam reforming can be interpreted by the preferable oxidation of Fe to Co. As mentioned above, in the case of the surface segregation of Co, when only the near-surface atoms are oxidized, the Fe/Co in the remaining metal particles can be increased. In contrast, when the oxidation proceeds up to the bulk of the metal particles, it is expected that the Fe species are more easily oxidized than the Co species based on the oxygen affinity. This tendency can decrease the Fe/Co ratio in the alloy phase by oxidation. The oxidation degree can influence the Fe/Co ratio of the Co–Fe alloy as well as the surface segregation.

The decrease of the peak intensity of the bcc Co–Fe alloy also supports the oxidation in the tar steam reforming. It has been known that the catalyst oxidation is one of the factors for the catalyst deactivation [42,70–74]. From the comparison between the activity and the structure after the reaction, in the steam reforming of toluene, the addition of H_2 to the reactant gas maintains the bcc Co–Fe alloy and high activity of toluene steam reforming. In the steam reforming of hydrocarbons, the ratio of the oxidation rate of active metal species to the reduction rate of oxidized species can determine the state of the metal species during the steady-state reaction conditions. In the toluene steam reforming without H_2 addition, the reduction rate with toluene is higher than the oxidation rate with steam for the fcc Co–Fe phase, however, the oxidation rate is higher for the bcc Co–Fe phase. When hydrogen was added to the reactant gas, the reduction rate is accelerated by this hydrogen and the bcc Co–Fe alloy phase is maintained in the metallic state and this causes high activity. In addition, in the case of the steam reforming of tar, it is thought that the tar contains more highly reactive components than toluene, suggesting that the reduction rate with tar can be much higher than that with toluene. This can be related to the presence of the bcc Co–Fe alloy phase after the reaction of the steam reforming of tar.

As a result, the bcc Co–Fe alloy phase can be a highly active species in the steam reforming. In addition, the bcc Co–Fe alloy phase was mainly formed on Co–Fe/Al_2O_3 (Fe/Co = 0.75 and 1.0) in Fig. 6 and Table 2. However, the activity of Co–Fe/Al_2O_3 (Fe/Co = 0.75 and 1.0) was lower than that of Co–Fe/Al_2O_3 (Fe/Co = 0.25). One possible explanation is the decrease of H_2 adsorption by the excess addition of Fe (Table 1). At the same time, the composition of Fe/Co in the bcc Co–Fe alloy phase increased significantly with increasing Fe content on Co–Fe/Al_2O_3. Too high Fe composition decreased the catalytic performance in the steam reforming and the H_2 adsorption amount, because the reforming activity of Fe itself is very low. Although Fe itself has very low reforming activity, the synergy between Co and Fe at the appropriate composition can increase the reforming activity and suppress the coke formation. This can be interpreted by the synergy between the activation of tar on the Co species and the supply of oxygen atom to the carbonaceous intermediate from neighboring Fe atoms, and the similar synergetic effect has been proposed on other systems using Ni–CeO_2, Ni–MnO_x, Ni–Fe catalysts in various reforming reactions [10,15,43].

4. Conclusions

1. The addition of Fe to Co/Al_2O_3 at the optimum amount enhanced the catalytic performance in the steam reforming of tar produced from the pyrolysis of cedar wood in terms of the catalytic activity and the suppression of coke deposition.
2. Catalyst characterization indicates that most Co and Fe species were reduced to form fcc Co–Fe and bcc Co–Fe alloy. The analysis of XRD indicates the ratio of Fe to Co in the bcc Co–Fe alloy phase was much higher than that in the fcc Co–Fe alloy phase.

3. The comparison of the catalytic performance in the toluene steam reforming without and with H_2 addition suggests that Co–Fe/Al_2O_3 (Fe/Co = 0.25) has high catalytic steam reforming activity.
4. The characterization of the catalyst after the catalytic use by means of XRD indicates that the bcc Co–Fe alloy particles tend to be oxidized more easily than the fcc Co–Fe alloy particles, although the bcc Co–Fe alloy at the suitable composition has high catalytic activity. The oxidation of the bcc Co–Fe alloy can explain the catalyst deactivation during the toluene steam reforming without H_2 addition.
5. The oxidation degree of the bcc Co–Fe alloy can be influenced by the ratio of the oxidation rate with steam to the reduction rate with hydrogen, biomass tar, and toluene.

Acknowledgement

This work was supported by the Cabinet Office, Government of Japan through it's "Funding Program for Next Generation World-Leading Researchers".

Appendix A. Supplementary data

Supplementary data associated with this article can be found, in the online version, at http://dx.doi.org/10.1016/j.apcatb.2012.03.025.

References

[1] G.W. Huber, S. Iborra, A. Corma, Chemical Reviews 106 (2006) 4044.
[2] A.V. Bridgwater, Applied Catalysis A: General 116 (1994) 5.
[3] H. de Lasa, E. Salaices, J. Mazumder, R. Lucky, Chemical Reviews 111 (2011) 5404.
[4] S. Sá, H. Silva, L. Brandão, J.M. Sousa, A. Mendes, Applied Catalysis B: Environmental 99 (2010) 43.
[5] J. Li, J. Liu, S. Liao, R. Yan, International Journal of Hydrogen Energy 35 (2010) 7399.
[6] T. Wang, J. Chang, X. Cui, Q. Zhang, Y. Fu, Fuel Processing Technology 87 (2006) 421.
[7] D.D. Le, X. Xiao, K. Morishita, T. Takarada, Journal of Chemical Engineering of Japan 42 (2009) 51.
[8] D. Wang, W. Yuan, W. Ji, Applied Energy 88 (2011) 1656.
[9] A. Corujo, L. Yermán, B. Arizaga, M. Brusoni, J. Castiglioni, Biomass and Bioenergy 34 (2010) 1695.
[10] K. Tomishige, T. Kimura, J. Nishikawa, T. Miyazawa, K. Kunimori, Catalysis Communications 8 (2007) 1074.
[11] T. Kimura, T. Miyazawa, J. Nishikawa, S. Kado, K. Okumura, T. Miyao, S. Naito, K. Kunimori, K. Tomishige, Applied Catalysis B: Environmental 68 (2006) 160.
[12] J. Nishikawa, K. Nakamura, M. Asadullah, T. Miyazawa, K. Kunimori, K. Tomishige, Catalysis Today 131 (2008) 146.
[13] J. Nishikawa, T. Miyazawa, K. Nakamura, M. Asadullah, K. Kunimori, K. Tomishige, Catalysis Communications 9 (2008) 195.
[14] K. Nakamura, T. Miyazawa, T. Sakurai, T. Miyao, S. Naito, N. Begum, K. Kunimori, K. Tomishige, Applied Catalysis B: Environmental 86 (2009) 36.
[15] M. Koike, C. Ishikawa, D. Li, L. Wang, Y. Nakagawa, K. Tomishige, Fuel in press http://dx.doi.org/10.1016/j.fuel.2011.04.009.
[16] D. Li, L. Wang, M. Koike, Y. Nakagawa, K. Tomishige, Applied Catalysis B: Environmental 102 (2011) 528.
[17] K. Urasaki, K. Tokunaga, Y. Sekine, M. Matsukata, E. Kikuchi, Catalysis Communications 9 (2008) 600.
[18] N. Iwasa, S. Masuda, N. Takezawa, Reaction Kinetics and Catalysis Letters 55 (1995) 349.
[19] T. Furusawa, A. Tsutsumi, Applied Catalysis A: General 278 (2005) 207.
[20] T. Furusawa, A. Tsutsumi, Applied Catalysis A: General 278 (2005) 195.
[21] K. Tasaka, T. Furusawa, A. Tsutsumi, Energy and Fuels 21 (2007) 590.
[22] K. Tasaka, T. Furusawa, A. Tsutsumi, Chemical Engineering Science 62 (2007) 5558.
[23] L. Wang, D. Li, M. Koike, H. Watanabe, Y. Xu, Y. Nakagawa, K. Tomishige, Fuel in press http://dx.doi.org/10.1016/j.fuel.2012.01.073.
[24] W.F. DeGroot, G.N. Richards, Fuel 67 (1988) 345.
[25] B. Zhang, X. Tang, Y. Li, Y. Xu, W. Shen, International Journal of Hydrogen Energy 32 (2007) 2367.
[26] X. Hu, G. Lu, Journal of Molecular Catalysis A: Chemical 261 (2007) 43.
[27] N. Iwasa, T. Yamane, M. Takei, J. Ozaki, M. Arai, International Journal of Hydrogen Energy 35 (2010) 110.
[28] L. He, H. Berntsen, E. Ochoa-Fernández, J. Walmsley, E. Blekkan, D. Chen, Topics in Catalysis 52 (2009) 206.
[29] A. Kazama, Y. Sekine, K. Oyama, M. Matsukata, E. Kikuchi, Applied Catalysis A: General 383 (2010) 96.
[30] J.A. Torres, J. Llorca, A. Casanovas, M. Domínguez, J. Salvadó, D. Montané, Journal of Power Sources 169 (2007) 158.
[31] V.A. de la Peña O'Shea, R. Nafria, P. Ramírez de la Piscina, N. Homs, International Journal of Hydrogen Energy 33 (2008) 3601.
[32] R. Nedyalkova, A. Casanovas, J. Llorca, D. Montané, International Journal of Hydrogen Energy 34 (2009) 2591.
[33] A. Casanovas, M. Roig, C. de Leitenburg, A. Trovarelli, J. Llorca, International Journal of Hydrogen Energy 35 (2010) 7690.
[34] X. Hu, G. Lu, Chemistry Letters 35 (2006) 452.
[35] M.M. Natile, F. Poletto, A. Galenda, A. Glisenti, T. Montini, L.D. Rogatis, P. Fornasiero, Chemistry of Materials 20 (2008) 2314.
[36] A.A. Mirzaei, A.B. babaei, M. Galavy, A. Youssefi, Fuel Processing Technology 91 (2010) 335.
[37] D.J. Duvenhage, N.J. Coville, Applied Catalysis A: General 153 (1997) 43.
[38] T. Ishihara, K. Eguchi, H. Arai, Applied Catalysis 30 (1987) 225.
[39] S. Lögdberg, D. Tristantini, Ø. Borg, L. Ilver, B. Gevert, S. Järås, E.A. Blekkan, A. Holmen, Applied Catalysis B: Environmental 89 (2009) 167.
[40] F. Tihay, A.C. Roger, A. Kiennemann, G. Pourroy, Catalysis Today 58 (2000) 263.
[41] K. Tomishige, Y. Himeno, Y. Matsuo, Y. Yoshinaga, K. Fujimoto, Industrial & Engineering Chemistry Research 39 (2000) 1891.
[42] Y. Chen, K. Tomishige, K. Yokoyama, K. Fujimoto, Applied Catalysis A: General 165 (1997) 335.
[43] L. Wang, D. Li, M. Koike, S. Koso, Y. Nakagawa, Y. Xu, K. Tomishige, Applied Catalysis A: General 392 (2011) 248.
[44] X-Ray Powder Diffraction Data File, ICDD 01-078-1970.
[45] X-Ray Powder Diffraction Data File, ICDD 01-089-8103.
[46] X-Ray Powder Diffraction Data File, ICDD 01-089-2355.
[47] X-Ray Powder Diffraction Data File, ICDD 00-022-1086.
[48] X-Ray Powder Diffraction Data File, ICDD 01-071-4409.
[49] X-Ray Powder Diffraction Data File, ICDD 01-077-7456.
[50] Q. Wang, Y. Cui, X. Yang, H. Yang, Journal of Materials Science—Materials in Electronics 20 (2009) 425.
[51] E. Jartych, J.K. Zurawicz, M. Budzynski, Journal of Physics: Condensed Matter 5 (1993) 927.
[52] Y. Yang, C. Jing, J.G. Yang, S.X. Cao, J.C. Zhang, Physica B 367 (2005) 61.
[53] P. Wetzel, P. Bertoncini, D. Berling, A. Mehdaoui, B. Loegel, D. Bolmont, G. Gewinner, C. Ulhaq-Bouillet, V. Pierron-Bohnes, Surface Science 499 (2002) 210.
[54] H. Moumeni, A. Nemamcha, S. Alleg, J.M. Grenèche, Materials Chemistry and Physics 122 (2010) 439.
[55] A.R. Denton, N.W. Ashcroft, Physical Review A 43 (1991) 3161.
[56] G.A. Prinz, Physical Review Letters 54 (1985) 1051.
[57] L.H. Bennett, B.C. Giessen, T.B. Massalski, Alloy Phase Diagrams, 1984.
[58] A.L. Patterson, Physical Review 56 (1939) 978.
[59] M.K. Niemelä, L. Backman, A.O.I. Krause, T. Vaara, Applied Catalysis A: General 156 (1997) 319.
[60] T.B. Reed, Free Energy Formation of Binary Compounds, MIT Press, Cambridge, MA, 1971, p. 66.
[61] H. Yang, R. Yan, H. Chen, D.H. Lee, C. Zheng, Fuel 86 (2007) 1781.
[62] D. Świerczyński, S. Libs, C. Courson, A. Kiennemann, Applied Catalysis B: Environmental 74 (2007) 211.
[63] O. Yamazaki, K. Tomishige, K. Fujimoto, Applied Catalysis A: General 136 (1996) 49.
[64] M. Nurunnabi, Y. Mukainakano, S. Kado, B. Li, K. Kunimori, K. Suzuki, K. Fujimoto, K. Tomishige, Applied Catalysis A: General 299 (2006) 145.
[65] Y. Chen, K. Tomishige, K. Yokoyama, K. Fujimoto, Journal of Catalysis 184 (1999) 479.
[66] M. Nurunnabi, K. Fujimoto, K. Suzuki, B. Li, S. Kado, K. Kunimori, K. Tomishige, Catalysis Communications 7 (2006) 73.
[67] M. Nurunnabi, S. Kado, K. Suzuki, K. Fujimoto, K. Kunimori, K. Tomishige, Catalysis Communications 7 (2006) 488.
[68] M. Nurunnabi, Y. Mukainakano, S. Kado, T. Miyazawa, K. Okumura, T. Miyao, S. Naito, K. Suzuki, K. Fujimoto, K. Kunimori, K. Tomishige, Applied Catalysis A: General 308 (2006) 1.
[69] M. Nurunnabi, Y. Mukainakano, S. Kado, T. Miyao, S. Naito, K. Okumura, K. Kunimori, K. Tomishige, Applied Catalysis A: General 325 (2007) 154.
[70] Y. Chen, O. Yamazaki, K. Tomishige, K. Fujimoto, Catalysis Letters 39 (1996) 91.
[71] Y. Matsuo, Y. Yoshinaga, Y. Sekine, K. Tomishige, K. Fujimoto, Catalysis Today 63 (2000) 439.
[72] M. Nurunnabi, B. Li, K. Kunimori, K. Suzuki, K. Fujimoto, K. Tomishige, Applied Catalysis A: General 292 (2005) 272.
[73] M. Nurunnabi, B. Li, K. Kunimori, K. Suzuki, K. Fujimoto, K. Tomishige, Catalysis Letters 103 (2005) 277.
[74] Y. Mukainakano, K. Yoshida, S. Kado, K. Okumura, K. Kunimori, K. Tomishige, Chemical Engineering Science 63 (2008) 4891.